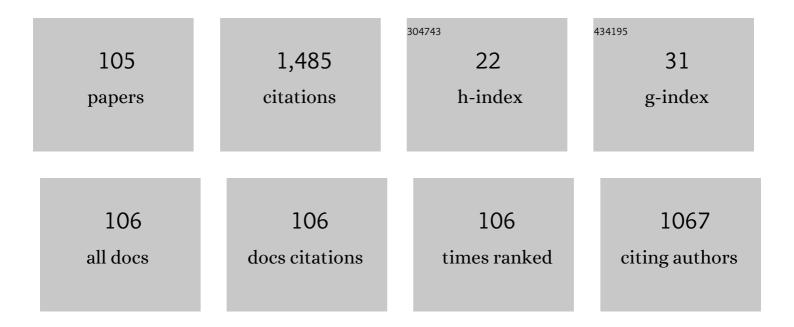
Heping Li

List of Publications by Year in descending order

Source: https://exaly.com/author-pdf/1347800/publications.pdf Version: 2024-02-01



#	Article	IF	CITATIONS
1	Design and Application of a Rock Porosity Measurement Apparatus under High Isostatic Pressure. Minerals (Basel, Switzerland), 2022, 12, 127.	2.0	3
2	First-Principles Calculations about Elastic and Li ⁺ Transport Properties of Lithium Superoxides under High Pressure and High Temperature. Chinese Physics Letters, 2022, 39, 026101.	3.3	2
3	Superionic iron alloys and their seismic velocities in Earth's inner core. Nature, 2022, 602, 258-262.	27.8	37

Raman Spectroscopic Studies of Pyrite at High Pressure and High Temperature. Minerals (Basel,) Tj ETQq0 0 0 rgBT Qverlock 10 Tf 50 6

7		2.0	2
5	Arsenopyrite oxidative dissolution in NaCl solution at high-temperature and high-pressure conditions: kinetics, pathways, dissolution mechanism and geological implications. Contributions To Mineralogy and Petrology, 2022, 177, .	3.1	0
6	High-pressure investigations on the isostructural phase transition and metallization in realgar with diamond anvil cells. Geoscience Frontiers, 2021, 12, 1031-1037.	8.4	8
7	Galena weathering in simulated alkaline soil: Lead transformation and environmental implications. Science of the Total Environment, 2021, 755, 142708.	8.0	7
8	Development of a 100 MPa water–gas two-phase fluid pressurization device. Acta Geochimica, 2021, 40, 25-31.	1.7	0
9	High-pressure structural phase transition and metallization in Ga ₂ S ₃ under non-hydrostatic and hydrostatic conditions up to 36.4 GPa. Journal of Materials Chemistry C, 2021, 9, 2912-2918.	5.5	20
10	Arsenopyrite weathering in acidic water: Humic acid affection and arsenic transformation. Water Research, 2021, 194, 116917.	11.3	26
11	<i>Ab initio</i> molecular dynamics investigation of the elastic properties of superionic <mml:math xmlns:mml="http://www.w3.org/1998/Math/MathML"><mml:mrow><mml:msub><mml:mi>Li</mml:mi><mml:m mathvariant="normal">O</mml:m </mml:msub></mml:mrow> under high temperature and pressure. Physical Review B, 2021, 103, .</mml:math 	n>25/mm	l:mp>
12	In situ electrical conductivity measurements of porous water-containing rock materials under high temperature and high pressure conditions in an autoclave. Review of Scientific Instruments, 2021, 92, 095104.	1.3	2
13	Electrical properties of dry polycrystalline olivine mixed with various chromite contents: Implications for the high conductivity anomalies in subduction zones. Geoscience Frontiers, 2021, 12, 101178.	8.4	7
14	Thermal Ionization of Hydrogen in Hydrous Olivine With Enhanced and Anisotropic Conductivity. Journal of Geophysical Research: Solid Earth, 2021, 126, e2021JB022939.	3.4	7
15	Arsenopyrite weathering in acid rain: Arsenic transfer and environmental implications. Journal of Hazardous Materials, 2021, 420, 126612.	12.4	19
16	Block and malleable arsenopyrite hot-pressure sintering: applied implications. Journal of Materials Research and Technology, 2020, 9, 8997-9003.	5.8	1
17	A simple and effective capsule sealing technique for hydrothermal experiments. American Mineralogist, 2020, 105, 1254-1258.	1.9	2
18	Anomalous elastic properties of superionic ice. Physical Review B, 2020, 102, .	3.2	7

#	Article	IF	CITATIONS
19	Effect of Chloride Ions on the Electrochemical Oxidation of Chalcopyrite at 340 °C and 21 MPa. Minerals (Basel, Switzerland), 2020, 10, 1071.	2.0	0
20	Electrochemical Study of Galena Weathering in NaCl Solution: Kinetics and Environmental Implications. Minerals (Basel, Switzerland), 2020, 10, 416.	2.0	4
21	Development of in-situ Micro-Raman spectroscopy system for autoclave experimental apparatus. Acta Geochimica, 2020, 39, 445-450.	1.7	0
22	In Situ Electrochemical Study of the Growth Kinetics of Passive Film on TC11 Alloy in Sulfate Solution at 300 ŰC/10 MPa. Materials, 2020, 13, 1135.	2.9	5
23	Electrical Conductivity of Clinopyroxeneâ€NaClâ€H 2 O System at High Temperatures and Pressures: Implications for Highâ€Conductivity Anomalies in the Deep Crust and Subduction Zone. Journal of Geophysical Research: Solid Earth, 2020, 125, e2019JB019093.	3.4	15
24	Arsenopyrite weathering in sodium chloride solution: Arsenic geochemical evolution and environmental effects. Journal of Hazardous Materials, 2020, 392, 122502.	12.4	14
25	The Phase Transition and Dehydration in Epsomite under High Temperature and High Pressure. Crystals, 2020, 10, 75.	2.2	11
26	Crystal structure of impurity-free rhodochrosite (MnCO3) and thermal expansion properties. Physics and Chemistry of Minerals, 2020, 47, 1.	0.8	14
27	Stability of copper acetate at high P-T and the role of organic acids and CO2 in metallic mineralization. Scientific Reports, 2020, 10, 5387.	3.3	0
28	An Overview of the Experimental Studies on the Electrical Conductivity of Major Minerals in the Upper Mantle and Transition Zone. Materials, 2020, 13, 408.	2.9	12
29	Study on properties of BaZr _{0.7} Ce _{0.2} Y _{0.1} O _{3â^îr} ceramics prepared by high-pressure sintering. Journal of the Ceramic Society of Japan, 2020, 128, 62-65.	1.1	3
30	Electrical conductivities of minerals and rocks in the Earth crust, upper mantle, mantle transition zone and subduction zone. Acta Geologica Sinica, 2019, 93, 120-121.	1.4	1
31	Characterization of metallization and amorphization for GaP under different hydrostatic environments in diamond anvil cell up to 40.0 GPa. Review of Scientific Instruments, 2019, 90, 066103.	1.3	24
32	Characterization of the pressure-induced phase transition of metallization for MoTe2 under hydrostatic and non-hydrostatic conditions. AIP Advances, 2019, 9, 065104.	1.3	15
33	Structural Phase Transition and Metallization of Nanocrystalline Rutile Investigated by High-Pressure Raman Spectroscopy and Electrical Conductivity. Minerals (Basel, Switzerland), 2019, 9, 441.	2.0	11
34	Thermal diffusivity and thermal conductivity of granitoids at 283–988 K and 0.3–1.5 GPa. American Mineralogist, 2019, 104, 1533-1545.	1.9	24
35	Pressure-induced phase transitions for goethite investigated by Raman spectroscopy and electrical conductivity. High Pressure Research, 2019, 39, 106-116.	1.2	13
36	Crystal structure of norsethite-type BaMn(CO3)2 and its pressure-induced transition investigated by Raman spectroscopy. Physics and Chemistry of Minerals, 2019, 46, 771-781.	0.8	8

#	Article	IF	CITATIONS
37	The influence of humic acids on the weathering of pyrite: Electrochemical mechanism and environmental implications. Environmental Pollution, 2019, 251, 738-745.	7.5	29
38	Effect of Temperature, Pressure, and Chemical Composition on the Electrical Conductivity of Schist: Implications for Electrical Structures under the Tibetan Plateau. Materials, 2019, 12, 961.	2.9	5
39	Evidences for phase transition and metallization in β-In2S3 at high pressure. Chemical Physics, 2019, 524, 63-69.	1.9	7
40	Phase Transition and Metallization of Orpiment by Raman Spectroscopy, Electrical Conductivity and Theoretical Calculation under High Pressure. Materials, 2019, 12, 784.	2.9	10
41	Influence of High Conductive Magnetite Impurity on the Electrical Conductivity of Dry Olivine Aggregates at High Temperature and High Pressure. Minerals (Basel, Switzerland), 2019, 9, 44.	2.0	14
42	Pressure-induced phase transitions of ZnSe under different pressure environments. AIP Advances, 2019, 9, .	1.3	21
43	Pressure-induced metallization in MoSe ₂ under different pressure conditions. RSC Advances, 2019, 9, 5794-5803.	3.6	26
44	Effect of temperature, pressure and chemical composition on the electrical conductivity of granulite and geophysical implications. Journal of Mineralogical and Petrological Sciences, 2019, 114, 87-98.	0.9	3
45	Li-ion battery material under high pressure: amorphization and enhanced conductivity of Li4Ti5O12. National Science Review, 2019, 6, 239-246.	9.5	49
46	Thermal Diffusivity of Lherzolite at High Pressures and High Temperatures Using Pulse Method. Journal of Earth Science (Wuhan, China), 2019, 30, 218-222.	3.2	3
47	Assessing the influence of humic acids on the weathering of galena and its environmental implications. Ecotoxicology and Environmental Safety, 2018, 158, 230-238. Pressure-induced irreversible metallization accompanying the phase transitions in <mml:math< td=""><td>6.0</td><td>14</td></mml:math<>	6.0	14
48	xmlns:mml="http://www.w3.org/1998/Math/MathML [*] > <mml:mrow><mml:mi mathvariant="normal">S<mml:msub><mml:mi mathvariant="normal">b<mml:mn>2</mml:mn></mml:mi </mml:msub><mml:msub><mml:mi mathvariant="normal">S<mml:mn>3</mml:mn></mml:mi </mml:msub></mml:mi </mml:mrow> .	3.2	45
49	Physical Review B, 2018, 97, . In Situ Electrochemical Investigation of Acidic Pressure Oxidation of Pyrite at 160–240°C. Journal of the Electrochemical Society, 2018, 165, C289-C294.	2.9	3
50	Deviatoric stresses promoted metallization in rhenium disulfide. Journal Physics D: Applied Physics, 2018, 51, 165101.	2.8	15
51	Limestone mechanical deformation behavior and failure mechanisms: a review. Acta Geochimica, 2018, 37, 153-170.	1.7	10
52	Migration of impurity level reflected in the electrical conductivity variation for natural pyrite at high temperature and high pressure. Physics and Chemistry of Minerals, 2018, 45, 85-92.	0.8	10
53	Single crystal growth, characterization and high-pressure Raman spectroscopy of impurity-free magnesite (MgCO3). Physics and Chemistry of Minerals, 2018, 45, 423-434.	0.8	17
54	An experimental study of interaction between pure water and alkaline feldspar at high temperatures and pressures. Acta Geochimica, 2018, 37, 60-67.	1.7	1

#	Article	IF	CITATIONS
55	High–pressure electrical conductivity and Raman spectroscopy of chalcanthite. Spectroscopy Letters, 2018, 51, 531-539.	1.0	5
56	In Situ Electrochemical Investigation of Pyrite Assisted Leaching of Chalcopyrite. Journal of the Electrochemical Society, 2018, 165, H813-H819.	2.9	7
57	Pressure-induced reversible metallization and phase transition in Zinc Telluride. Modern Physics Letters B, 2018, 32, 1850342.	1.9	6
58	Phase Transition and vibration properties of MnCO3 at high pressure and high-temperature by Raman spectroscopy. High Pressure Research, 2018, 38, 212-223.	1.2	19
59	Effect of chemical composition on the electrical conductivity of gneiss at high temperatures and pressures. Solid Earth, 2018, 9, 233-245.	2.8	10
60	Effect of dehydrogenation on the electrical conductivity of Fe-bearing amphibole: Implications for high conductivity anomalies in subduction zones and continental crust. Earth and Planetary Science Letters, 2018, 498, 27-37.	4.4	55
61	Single-crystal elasticity of the rhodochrosite at high pressure by Brillouin scattering spectroscopy. High Pressure Research, 2018, 38, 396-405.	1.2	1
62	Single crystal growth, crystalline structure investigation and high-pressure behavior of impurity-free siderite (FeCO3). Physics and Chemistry of Minerals, 2018, 45, 831-842.	0.8	13
63	Pressure-induced structural phase transition and dehydration for gypsum investigated by Raman spectroscopy and electrical conductivity. Chemical Physics Letters, 2018, 706, 151-157.	2.6	11
64	Rapid mass production of novel 3D Cu@CuI coreâ€shell mesh as highly flexible and efficient photocatalyst. Journal of the American Ceramic Society, 2018, 101, 5781-5790.	3.8	3
65	Effect of dehydration on the electrical conductivity of phyllite at high temperatures and pressures. Mineralogy and Petrology, 2017, 111, 853-863.	1.1	14
66	Structural stability and Li-ion transport property of LiFePO4 under high-pressure. Solid State Ionics, 2017, 301, 133-137.	2.7	25
67	High-pressure and high-temperature Raman study of cinnabar. Spectroscopy Letters, 2017, 50, 342-346.	1.0	0
68	Anomalous phase transition of Bi-doped Zn2GeO4 investigated by electrical conductivity and Raman spectroscopy under high pressure. Journal of Applied Physics, 2017, 121, 125901.	2.5	12
69	Influence of dehydration on the electrical conductivity of epidote and implications for highâ€conductivity anomalies in subduction zones. Journal of Geophysical Research: Solid Earth, 2017, 122, 2751-2762.	3.4	45
70	Pressure-induced permanent metallization with reversible structural transition in molybdenum disulfide. Applied Physics Letters, 2017, 110, .	3.3	45
71	SrB ₄ O ₇ :Sm ²⁺ : an optical sensor reflecting non-hydrostatic pressure at high-temperature and/or high pressure in a diamond anvil cell. High Pressure Research, 2017, 37, 18-27.	1.2	15
72	Novel heterostructured InN/TiO ₂ submicron fibers designed for high performance visible-light-driven photocatalysis. Catalysis Science and Technology, 2017, 7, 5105-5112.	4.1	24

#	Article	IF	CITATIONS
73	A novel experimental device for electrochemical measurements in supercritical fluids up to 700 °C/1000 bar and its application in the corrosion study of superalloy Inconel 740H. RSC Advances, 2017, 7, 33914-33920.	3.6	8
74	Pyrite oxidation under simulated acid rain weathering conditions. Environmental Science and Pollution Research, 2017, 24, 21710-21720.	5.3	19
75	Electrical conductivity of mudstone (before and after dehydration at high P-T) and a test of high conductivity layers in the crust. American Mineralogist, 2017, 102, 2450-2456.	1.9	16
76	Pressure-induced irreversible amorphization and metallization with a structural phase transition in arsenic telluride. Journal of Materials Chemistry C, 2017, 5, 12157-12162.	5.5	35
77	Experimental Study on the Electrical Conductivity of Pyroxene Andesite at High Temperature and High Pressure. Pure and Applied Geophysics, 2017, 174, 1033-1041.	1.9	6
78	Influence of temperature, pressure, and oxygen fugacity on the electrical conductivity of dry eclogite, and geophysical implications. Geochemistry, Geophysics, Geosystems, 2016, 17, 2394-2407.	2.5	35
79	Raman scattering of 2 <i>H</i> -MoS2 at simultaneous high temperature and high pressure (up to 600 K) Tj ETQq1	1 0.7843 1.3	14 rgBT /0\
80	Firstâ€principles prediction of fast migration channels of potassium ions in KAlSi ₃ O ₈ hollandite: Implications for high conductivity anomalies in subduction zones. Geophysical Research Letters, 2016, 43, 6228-6233.	4.0	16
81	Influence of pH, Pb2+, and temperature on the electrochemical dissolution of galena: environmental implications. Ionics, 2016, 22, 975-984.	2.4	7
82	The influence of calcium fluoride on the electrochemical dissolution of chalcopyrite in sulfuric acid solution. Ionics, 2015, 21, 749-753.	2.4	2
83	Dependence of R fluorescence lines of rubies on Cr ³⁺ concentration at various temperatures, with implications for pressure calibrations in experimental apparatus. American Mineralogist, 2015, 100, 1554-1561.	1.9	1
84	Modeling geochemical factors controlling fluoride concentration in groundwater. Arabian Journal of Geosciences, 2015, 8, 9133-9147.	1.3	9
85	Temperature and pressure dependence of electrical conductivity in synthetic anorthite. Solid State lonics, 2015, 276, 136-141.	2.7	22
86	Influence of temperature, pressure, and chemical composition on the electrical conductivity of granite. American Mineralogist, 2014, 99, 1420-1428.	1.9	29
87	Electrochemical behavior of pyrite in acidic solution with different concentrations of NaCl. Diqiu Huaxue, 2014, 33, 374-381.	0.5	2
88	The temperature dependence of thermal conductivity for lherzolites from the North China Craton and the associated constraints on the thermodynamic thickness of the lithosphere. Geophysical Journal International, 2014, 197, 900-909.	2.4	15
89	Electrical conductivity of K-feldspar at high temperature and high pressure. Mineralogy and Petrology, 2014, 108, 609-618.	1.1	28
90	Electrical conductivity of alkali feldspar solid solutions at high temperatures and high pressures. Physics and Chemistry of Minerals, 2013, 40, 51-62.	0.8	38

#	Article	IF	CITATIONS
91	Electrical conductivity of Alm82Py15Grs3 almandine-rich garnet determined by impedance spectroscopy at high temperatures and high pressures. Tectonophysics, 2013, 608, 1086-1093.	2.2	24
92	Influence of differential stress on the galvanic interaction of pyrite–chalcopyrite. Ionics, 2013, 19, 77-82.	2.4	3
93	The effect of chemical composition and oxygen fugacity on the electrical conductivity of dry and hydrous garnet at high temperatures and pressures. Contributions To Mineralogy and Petrology, 2012, 163, 689-700.	3.1	50
94	Electrical conductivity of albite at high temperatures and high pressures. American Mineralogist, 2011, 96, 1821-1827.	1.9	29
95	A comparison of the electrochemical behaviors of pyrite and chalcopyrite in a NaCl solution at room temperature and under differential stress. Minerals Engineering, 2010, 23, 691-697.	4.3	6
96	Anisotropy of synthetic quartz electrical conductivity at high pressure and temperature. Journal of Geophysical Research, 2010, 115, .	3.3	23
97	The electrical conductivity of dry polycrystalline olivine compacts at high temperatures and pressures. Mineralogical Magazine, 2010, 74, 849-857.	1.4	36
98	The electrical conductivity of upper-mantle rocks: water content in the upper mantle. Physics and Chemistry of Minerals, 2008, 35, 157-162.	0.8	36
99	Experimental study of grain boundary electrical conductivities of dry synthetic peridotite under highâ€ŧemperature, highâ€pressure, and different oxygen fugacity conditions. Journal of Geophysical Research, 2008, 113, .	3.3	40
100	Mixed potential oscillations in the dissolution of galena in ferric sulfate solution. Mining, Metallurgy and Exploration, 2008, 25, 211-214.	0.8	0
101	Temperature dependence of the first pressure derivative of the isothermal bulk modulus for solid materials at zero pressure: Application to MgO. Journal of Geophysical Research, 2005, 110, .	3.3	6
102	New technique to controlin situ oxygen fugacity in water-free high-pressure system. Science Bulletin, 1998, 43, 1353-1358.	1.7	0
103	In situcontrol of oxygen fugacity at high temperature and high pressure: A Ni-O system. Geophysical Research Letters, 1998, 25, 817-820.	4.0	11
104	New Technique to In situ Control Oxygen Fugacity in Water-free High Pressure System Review of High Pressure Science and Technology/Koatsuryoku No Kagaku To Gijutsu, 1998, 7, 1523-1525.	0.0	0
105	Pressure measurement using the <i>R</i> fluorescence peaks and 417Âcm ^{â^1} Raman peak of an anvil in a sapphire-anvil cell. High Pressure Research, 0, , 1-10.	1.2	2

7